laterally shifted self-interference (see the figure for the $L = \hbar$ beam).

A compact source of optical vortex beams requires a minute detector. Ji *et al.* realized a previously unappreciated photogalvanic effect (*14*) to enable direct on-chip electrical readout of orbital angular momentum in an optical vortex beam. This effect bears a similarity to the photon drag effect (*15*), where the linear momentum of absorbed photons is transferred to charge carriers. The difference between the two effects can be readily understood from the twisted bundle of rays: The demonstrated photogalvanic effect would vanish if each ray were independent, whereas the photon drag effect would be unaffected. The helical phase gradient of the optical beam leads to a photocurrent proportional to L, which is governed by the fourth-order conductivity tensor. Ji *et al.* fabricated electrodes of various shapes on tungsten ditelluride, a room-temperature Weyl semimetal with broken inversion symmetry, for use as photocurrent detectors. They found that the photocurrent displayed steplike changes with L, from which the contribution due to spin angular momentum was also eliminated reliably.

These two demonstrations provide a robust platform from which to scale down the footprint of optical vortex laser generation and detection, which so far rely largely on traditional bulk and fiber optical elements (*2*, *5*). Switching the angular momentum directly from the source opens new opportunities in signal multiplexing and modulation in telecommunications. A potential issue is the orthogonality of multiple signal channels: Switching from a spin-orbital correlated state to a vector vortex beam polarized in the radial or azimuthal direction is similar to switching from circular polarization to linear polarization. Whether single photons with orbital angular momentum can be generated and measured on this platform awaits further investigation of the possibilities for its application in quantum information processing. ■

REFERENCES AND NOTES

1. A. A. Abrikosov, *Rev. Mod. Phys.* **76**, 975 (2004).
2. M. Padgett, J. Courtial, L. Allen, *Phys. Today* **57**, 35 (May 2004).
3. Z. Zhang *et al.*, *Science* **368**, 760 (2020).
4. Z. Ji *et al.*, *Science* **368**, 763 (2020).
5. B. Ndagano, I. Nape, M. A. Cox, C. Rosales-Guzman, A. Forbes, *J. Lightwave Technol.* **36**, 292 (2018).
6. Z. Shao, J. Zhu, Y. Chen, Y. Zhang, S. Yu, *Nat. Commun.* **9**, 926 (2018).
7. N. Carlon Zambon *et al.*, *Nat. Photonics* **13**, 283 (2019).
8. X. Cai *et al.*, *Science* **338**, 363 (2012).
9. H. Cao, J. Wiersig, *Rev. Mod. Phys.* **87**, 61 (2015).
10. P. Miao *et al.*, *Science* **353**, 464 (2016).
11. Q. T. Cao *et al.*, *Phys. Rev. Lett.* **118**, 033901 (2017).
12. C. Huang *et al.*, *Science* **367**, 1018 (2020).
13. N. Hatano, D. R. Nelson, *Phys. Rev. Lett.* **77**, 570 (1996).
14. G. F. Quinteiro, P. I. Tamborenea, *Europhys. Lett.* **85**, 47001 (2009).
15. P. N. Lebedew, *Ann. Phys.* **6**, 433 (1901).

ACKNOWLEDGMENTS

Supported by NSF grant PHY-1847240.

10.1126/science.abb8091

On-chip generation and detection of twisted light

Zhang *et al.* and Ji *et al.* developed chip-scale methods to generate and detect optical vortex beams.

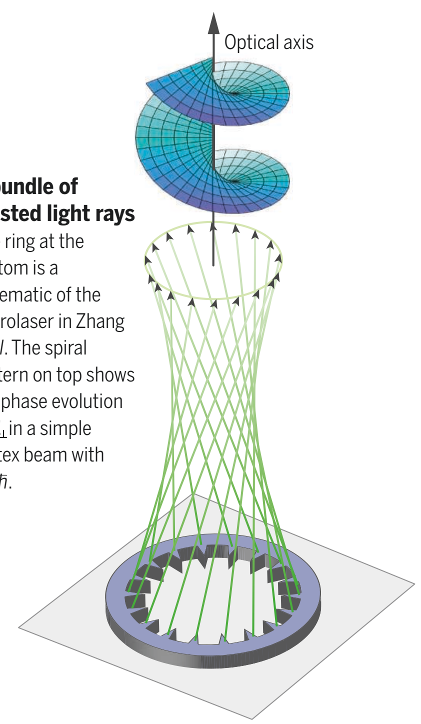

A bundle of twisted light rays
The ring at the bottom is a schematic of the microlaser in Zhang *et al.* The spiral pattern on top shows the phase evolution of $\mathbf{E}_\perp$ in a simple vortex beam with $L = \hbar$.

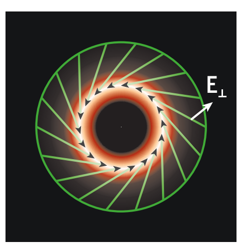

View from the optical axis at half height of the twisted bundle
The donut-shaped beam pattern and the direction of the transverse electric field are superposed.

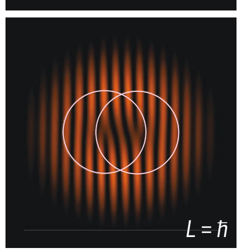

Pitchforks formed in self-interference
The two circles illustrate the lateral shift of the same vortex beam.

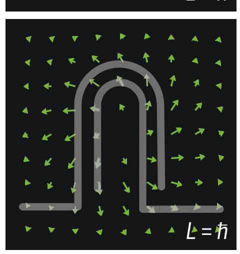

Vortex detection
Photocurrent (green arrows) is generated by the helical phase of an optical vortex beam and the collecting electrodes used by Ji *et al.*

GRAPHIC: ADAPTED BY N. CARY/SCIENCE

GEOPHYSICS

Seismicity from the deep magma system

Deep seismicity may reflect magma cooling beneath volcanoes

By **Robin S. Matoza**

A systematic scan of seismic waveform archives on the Island of Hawai'i has revealed subtle but persistent near-periodic pulses originating within the deep magma plumbing system of Mauna Kea, a dormant volcano that last erupted ~4500 years ago. On page 775 of this issue, Wech *et al.* (*1*) report the detection of over a million of the deep (22 to 25 km below sea level) long-period seismic events, which have been occurring continuously and repetitively, often with precise regularity (every ~7 to 12 min), for at least 18 years. This discovery offers new views into the origin of this mysterious type of deep volcanic seismicity.

Seismic data form the backbone of most volcano monitoring networks and play a critical role in understanding how volcanoes work. Volcanic seismicity includes volcano-tectonic (VT) earthquakes (ordinary brittle-failure earthquakes driven by magmatic stresses) and long-period [(LP), 0.5 to 5 Hz] seismicity (volcanic seismicity that is thought to actively involve a fluid in the source mechanism) (*2*). LP seismicity includes individual transient LP events and sustained volcanic tremor signals. LP seismicity at shallow depth (<3 km) in a volcanic edifice is commonly explained by the excitation and resonance of fluid-filled cracks associated with magmatic-hydrothermal interactions or magmatic degassing and is a characteristic signature of unrest and eruption (*3*). Precise regularity in sustained sequences of shallow LP seismicity has been documented at numerous volcanoes worldwide (*2*).

In the roots of volcanic systems below this shallow activity, seismicity extends down to mantle depths (to ~60 km), but linking seismicity to magma pathways is not straight-

Department of Earth Science and Earth Research Institute, University of California, Santa Barbara, CA, USA. Email: rmatoza@ucsb.edu

forward. Deep long-period (DLP) seismicity has been observed at depths of 10 to 60 km beneath volcanoes in a range of tectonic settings and has generally been attributed to magma transport in the mid-to-lower crust and uppermost mantle (*2*). The idea that DLP seismicity may represent cooling of magma stalled near the Moho (crust-mantle boundary) has also been proposed (*4*). However, compared to shallow LP seismicity, DLP seismicity is relatively understudied and poorly quantified, largely owing to difficulties in detecting these weak signals in the background noise (*5*).

Typically, much of the proposed deep magma transport system appears aseismic, inferred as relatively open flow channels in which quasi-steady magma flow does not generate seismicity (*6*). For example, beneath the active volcanoes on the Island of Hawaiʻi (an oceanic hotspot), deep (>10 km) and intermediate depth (5 to 15 km) LP seismicity, including deep harmonic tremor, has been recorded for decades at Kīlauea (*6*, *7*), and occasional DLP swarms (sequences of repetitive events closely clustered in time and space) have occurred beneath Mauna Loa (*8*). Precise relocation of this repetitive DLP seismicity collapses it to markedly consistent and small source volumes along the presumed magma ascent paths (*7*, *8*). This repeated seismic illumination of only a tiny portion of the inferred magma transport system over decades of eruptive changes indicates a source process controlled by stable geologic or magma pathway structure, such as a geometrical conduit discontinuity or a particularly strong barrier to magma flow (*6*, *7*, *8*). A more complex picture has recently emerged at Mammoth Mountain, California, with swarms of DLPs clustering in the middle and top of a relatively aseismic zone between two arms of migrating brittle-failure earthquakes (*9*).

DLP seismicity is challenging to detect with standard seismic network processing and typical noise conditions and is likely underreported, but DLPs have been identified in multiple tectonic settings located at mid-to-lower crustal depths, with most appearing to represent a relatively stable background process (*5*, *10*, *11*). Between 1989 and 2002, 162 DLPs were detected beneath 11 volcanic centers in the Aleutian arc, occurring both in isolation and as event sequences lasting from 1 to 30 min (*10*). Between 1980 and 2009, more than 60 DLPs were identified beneath six Cascades volcanic centers, none directly related to volcanic activity (*11*). DLPs occur beneath each of the major volcanic centers in Northern California (*5*). Given the low signal-to-noise ratios of most DLP observations, source mechanism studies have rarely been attempted. Analyses of DLPs at Iwate, Japan, produced variable mechanisms, suggesting a complex magma system at the source region (*12*).

Origin of deep long-period seismicity

Inactive volcanoes can exhibit deep long-period (DLP) seismicity. This activity may arise from pooled, cooling magma at the base of Earth's crust. Magmatic gases exsolve from this pool as the magma crystallizes. Protraction of this "second boiling" is linked to DLP activity.

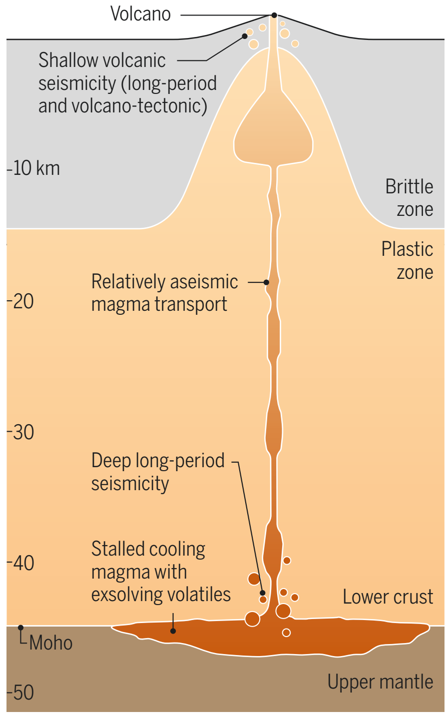

GRAPHIC: V. ALTOUNIAN/*SCIENCE*

The 1991 eruption of Pinatubo, Philippines, provided new observations connecting DLPs with deep magma transport in a subduction setting and identified DLPs as potentially important eruption precursors (*13*). Prior to the 15 June 1991 eruption, about 400 DLPs were observed between late May and early June 1991, along with >25 hours of low-amplitude DLP tremor in 1- to 10-hour-long episodes (*13*). The DLPs were located at 28- to 40-km depth at the base of the crust below Pinatubo and were temporally correlated with surficial changes and shallow seismicity. The DLP seismicity preceded, by about 1 to 4 hours, shallow (<3 km depth) LP events, tremor, and steam emissions. DLP seismicity increased a few days before the extrusion of an andesitic (volcanic rock type of intermediate silica content, commonly associated with subduction zones) dome containing inclusions of freshly quenched olivine basalt and was accordingly interpreted as resulting from deep basaltic fluid injections into the base of the magma chamber (*13*). A similar increase in mid-to-lower crustal DLP seismicity occurred about 10 months before the 1999 eruption of Shishaldin, Alaska; conversely, 1992 eruptions of Mount Spurr, Alaska, initiated DLP seismicity (*10*).

Waveform template matching greatly enhances the detection of DLP seismicity, allowing a more complete investigation of these spatiotemporal relations (*14*, *15*). Results from applying this method to 2011–2012 activity at the Klyuchevskoy volcanic group in Kamchatka, Russia, supported the notion that DLP seismicity may (at least in some cases) represent an early eruption precursor and identified systematic connections between deep and shallow LP seismicity and eruptions at multiple volcanoes (*14*). A recent longer study of 17 years of seismicity at Hakone, Japan, reveals similar patterns, with DLPs repeatedly preceding inflation of the volcanic edifice and shallow VT seismicity, and in one case, a phreatic eruption (*15*).

The detection of over a million DLPs by Wech *et al.* is an impressive demonstration of this technique, but as the authors point out, the occurrence of such a prolific number of these events beneath dormant Mauna Kea is surprising. The resulting hypothesis that some (or perhaps millions of) DLPs are related to crystallization-induced degassing ("second boiling") of stagnant cooling magma (see the figure) should be tested at other volcanoes in different tectonic settings worldwide. ■

REFERENCES AND NOTES

1. A. G. Wech, W. A. Thelen, A. M. Thomas, *Science* **368**, 775 (2020).
2. B. A. Chouet, R. S. Matoza, *J. Volcanol. Geotherm. Res*. **252**, 108 (2013).
3. B. A. Chouet, *Nature* **380**, 309 (1996).
4. N. Aso, V. Tsai, *J. Geophys. Res.* **119**, 8442 (2014).
5. A. M. Pitt, D. P. Hill, S. W. Walter, M. J. S. Johnson, *Seismol. Res. Lett*. **73**, 144 (2002).
6. K. Aki, R. Koyanagi, *J. Geophys. Res.* **86**, 7095 (1981).
7. R. S. Matoza, P. M. Shearer, P. G. Okubo, *Geophys. Res. Lett*. **41**, 3413 (2014).
8. P. G. Okubo, C. J. Wolfe, *J. Volcanol. Geotherm. Res.* **178**, 787 (2008).
9. A. J. Hotovec-Ellis *et al*., *Sci. Adv*. **4**, eaat5258 (2018).
10. J. A. Power, S. D. Stihler, R. A. White, S. C. Moran, *J. Volcanol. Geotherm. Res*. **138**, 243 (2004).
11. M. L. Nichols, S. D. Malone, S. C. Moran, W. A. Thelen, J. E. Vidale, *J. Volcanol. Geotherm. Res*. **200**, 116 (2011).
12. H. Nakamichi *et al*., *Geophys. J. Int*. **154**, 811 (2003).
13. R. A. White, in Fire and mud, eruptions and lahars of Mount Pinatubo, Philippines, C. G. Newhall, R. S. Punongbayan, Eds. (Univ. of Washington Press, 1996), pp. 307–328.
14. N. M. Shapiro *et al*., *Nat. Geosci*. **10**, 442 (2017).
15. Y. Yukutake, Y. Abe, R. Doke, *Geophys. Res. Lett*. **46**, 11035 (2019).

ACKNOWLEDGMENTS

R.S.M. received support from NSF grants EAR-1446543 and EAR-1847736.

10.1126/science.abc2452